Cancer Research and Biological Therapeutics
Volume 1, Issue 1, 2026, Pages 1–18

RESEARCH ARTICLE

Targeting Progesterone Receptor in Breast Cancer: Computational and Experimental Insights into the Role of Pterocarpus marsupium and Naringetol

Natarajan Kiruthiga[1], Vijayakumar Murugesan[2], Kommu Pradeep[3], Jayashree Venugopal[4], Mangirish Deshpande[5*]

Breast cancer is still one of the top causes of death globally, and it requires coming up with safer and efficient drugs in terms of treatment. This paper examines the possibility of natural bioactive compounds, Rubia cordifolia and *Naringetol*, as complementary agent to standard therapeutic procedure of breast cancer. Machine learning models were constructed as predictive models using molecular interactions of these compounds, evaluated against the Progesterone receptor (PR) with molecular docking and dynamic calculations to allow their bioactivity assessment. The Random Forest appeared the strongest among the tested machine learning models in that it had a predictive accuracy of 78.12% which provides a good indication that Random Forest can be used to predict bioactivity. Moreover, in silico predictions also found *Naringetol* and Propterol-B to be potential bioactivities against PR. Proteins PGR, MAPK, and BRCA1 were also found to play an important role in pathways related to cancer, indicating that they can be used as targets of the therapy. Molecular docking indicated high binding energies of *Naringetol* to PR, which was supported by the constant values of RMSD and RMSF during the molecular dynamics analysis. The pharmacokinetic profiles turned out to be promising, with positive results during the ADMET analysis, in terms of good absorption and low risk of toxicity, which makes *Naringetol* a promising candidate to continue developing as a drug. Moreover, the SLNs, in which *Naringetol* was encapsulated, revealed the mainly positive data regarding their release kinetics, and stability at physiological environments, as the drug was presented in the sustained manner at pH 7.7. The *in vitro* MTT Analysis revealed that *Naringetol* had considerable anticancer activity at high doses as it demonstrated dose-dependent cytotoxicity. These results all warrant the view that a combination of natural compounds and the current therapeutic methods regarding breast cancer is, in fact, viable and would, through such a combination, lead to a safer and more successful treatment method.

Keywords: Breast cancer; Natural bioactive compounds; Progesterone receptor; Machine learning; Molecular docking; Naringetol; SLNs

*Corresponding authors
Dr. Mangirish Deshpande ✉: mangirishd@gmail.com
*Co-authors
Natarajan Kiruthiga: kiruthigagovindaraj@gmail.com
Vijayakumar Murugesan: vijay.lithu17@gmail.com
Jayashree Venugopal mailtovjayashree@gmail.com
Kommu Pradeep: kommu.pradeep@gmail.com
[1]Department of Pharmaceutical Chemistry, KMCH college of Pharmacy, Kalappatti road, Coimbatore, Tamil Nadu 641048, India
[2]Department of Pharmaceutics, School of Pharmacy, JSS Academy of Higher Education and Research, Mauritius
[3]Faculty of Health Sciences, Villa College, Boduthakurufaanu Magu, Malé, Maldives
[4]Department of Pharmacology, School of Pharmaceutical Sciences, Vels Institute of Science, Technology & Advanced Studies, Pallavaram, Chennai, Tamil Nadu 600117, India
[5*]Department of Pharmacology, PES'S Rajaram and Tarabai Bandekar College of Pharmacy, Ponda-403401, Goa, India

1 Introduction

Cancer remains to be among the major forms of morbidity and mortality in the world with an estimated 9.6 million deaths in the year 2018 reported worldwide. Breast cancer stands out among the many other forms of cancer since it is both widespread and creates an impression on women. The World Health Organization (WHO) notes that breast cancer is the most diagnosed cancer in the globe and it is the second major killer of cancer-related deaths in females. Although considerable progress is gained in the diagnosis and treatment of breast cancer the complexity of the disease, molecular heterogeneity, and development of resistance to conventional therapies remain a concern to modern medicine (1, 2). Breast cancer is multi-factorial in nature and this occurs because of genetic, environmental, and lifestyle factors. Detection and early treatment are the most important in enhancing survivals. Traditional treatment approaches like chemotherapy, radiations and surgery have really changed the outcome to many patients by expanding their prognosis with many years to live. These interventions, however, are usually coupled with some severe side effects whereas the quality of life reduces. A number of breast cancer subtypes, including triple-negative breast cancer (TNBc), do not respond to standard treatment methods, which means there is a dire need in novel types of treatment methods. Such is the case that is why alternative therapies should be developed, especially that which could be able to provide both effectiveness and less toxicity (3, 4). The bioactive content found in natural products has attracted enormous research to be conducted on them as they have shown potential to prevent growth of cancer

cells, trigger apoptosis and make tumors susceptible to conventional therapies. A large number of natural products that are plant based have shown to possess anticancer activities, due to the ability to interact with the different pathways that are involved in cancer development. These bioactive compounds are a promise in lieu of use of synthetic drugs since they mostly have fewer side effects and have the capacity to target several points at a go and hence believes to take the ideal form of combination therapy. In this regard, *Pterocarpus marsupium*, a medicinal plant has come into view as a possible source of therapeutic skin developing agents of breast cancer (5, 6). *Pterocarpus marsupium* as an Indian Kino tree has traditional application of its anti-inflammatory effects, anticancer as well as antioxidant properties explained in Ayurvedic medicine. It has been reported that there is a considerable antiproliferation property of the extracts of Pterocarpus marsupium substance on different cancer cell lines such as the breast cancer, having an influence on some of the key molecular pathways, namely apoptosis, cell cycle arrest, and angiogenesis. The biologically active components found in Pterocarpus marsupium have a potential of being used as cancer cell growth inhibitors and hence a good compound worth exploring in cancer treatment purposes (7-12). *Naringetol*, a flavonoid extractable in citrus fruits and additional shrubs, is another hopeful natural compound. *Naringetol* has been demonstrated to have great anticancer effects, especially on breast cancer, including apoptosis induction, cell cycle arrest, metastatic inhibition. It is reported to affect the most important molecular pathway of signaling such as oxidative stress, inflammation and cell survival. It is evident that *Naringetol* has potential to treat breast cancer through combination therapy since it alters these pathways (13-15). Natural products have been found to not only have an effect of treating cancerous breast cells, but also an enhancement of the effect of previously used drugs which include chemotherapy and targeted therapy drugs. Natural compounds such as those found in Pterocarpus marsupium and *Naringetol* are effective in managing holistic treatment of cancer because it eliminates the resistance remarks and improves the side effects of the traditional treatment methods (16-20). *Naringetol* is an historically used or a tested lethal drug but is also undergoing trial to ascertain the anticancer effect. Studies had shown that *Naringetol* is cytotoxic in various cancer cell lines including breast cancer cells by inducing apoptosis and arrest in cell cycle. It is also presupposed that molecular action, which the substance undergoes, can be associated with its activity to prevent the growth of cancer cells by preventing the entry of important signaling molecules and cell proteins (21, 22). Natural products such as *Naringetol* combined with the standard agent of chemotherapy have shown potential of strengthening the undertakings of cancer treatment given minimal side effects. These are naturally occurring compounds, which may propose a comprehensive approach to the treatment of breast cancer that would complement the treatment profile of the synthetic drugs (23, 24). The aim of the research is to study therapeutic potential of Pterocarpus marsupium and *Naringetol* in breast cancer with regard to their molecular mechanism of action, including induction of apoptotic cell death, prevention of cell division, and regulation of important signaling pathways involved in breast cancer development. Moreover, the given study will compare the synergetic actions between these natural compounds used along with standard breast cancer treatment, trying to discover the possibility of their complement to therapies and diminishing the side effects. This endeavor has aimed to determine Pterocarpus marsupium and *Naringetol* as a potential candidate in the development of new safer and better treatment methods to deal with breast cancer through computer and experimentation analysis.

1.1 Materials and Methods

1.1.1 Dataset Collection

In this work the data provided by the BindingDB database, which is a longstanding and established database that contains extensive records of chemical compounds that have been reported to bind the Protein Progesterone receptor (PR), was used. The dataset was curated specifically through the choice of target compounds, the affinity of which with the PR was known. The records of each of the compounds were uniquely identifiable through monomer names, SMILES (Simplified Molecular Input Line Entry System) structures, and IC_{50} values, which were determined in nanomolar (nM) concentrations. In order to simplify the creation of predictive models, IC_{50} values were made in terms of negative values of logarithm, which is known as pIC_{50} values. Strict checks concerning cheminformatics were made with the help of the tools like RDKit and Open Babel to make sure that the results are chemically viable. Structurally inconsistent compound or compound with invalid SMILES were not included in the dataset. Also, a complete set of molecular descriptors was computed with Mordred descriptor generator, and a detailed list of the structural and physicochemical properties was obtained on each compound. (25-28) The compounds were divided into three groups with reference to pIC 50 values: pIC_{50}: least active ($pIC_{50} \leq 5.0$), moderately active ($5.0 < pIC_{50} \leq 7.0$), and active ($pIC_{50} > 7.0$).

1.1.2 Data Preprocessing and Feature Selection for Machine Learning Modeling

To make the dataset ready and able to be used in machine learning analysis, the dataset was subjected to an elaborate preprocessing pipeline process. First of all, the presence or absence of values present on the data was counted and the incomplete or missing values were dropped to preserve the integrity and completeness of the data. The filtering was done with a constant filter, which was done in order to remove the features that had no variance and the features that had a low variance (less than a value of 0.01), since they were not considered to carry sufficient information to discriminate between the bioactivities of compounds. Multicollinearity could be solved by eliminating the descriptors having a large Pearson correlation coefficient of more than 0.75 to still obtain information that was unique. Z-scores were used to find out how many outliers there were, and the data points outside the range of +/- 7 were removed. This was followed by ranking of descriptors based on their importance when classifying the progesterone receptor bioactivity only keeping the best descriptors with maximum information. The last dataset was split into training and testing portions in the proportion of 70:30, which allowed training and testing the model robustly.

1.1.3 Model Building

Multiple and various machine learning algorithms were used to create classification models classifying the bioactivity of the compounds toward the Progesterone receptor. The models applied on the present study were Random Forest, Instance-Based k-Nearest Neighbor (IBK), Multilayer Perceptron, Decision Tree, Logistic Regression, Sequential Minimal Optimization (SMO), Kstar, and Naive Bayes. All the algorithms were implemented in the WEKA software that is known to be a powerful software library with diverse data mining and classification capabilities. The evaluation of the models was done using several statistical measures such as accuracy, Kappa statistic, Mean Absolute Error (MAE), Root Mean Squared Error (RMSE), Relative Absolute Error (RAE), and Root Relative Squared Error (RRSE). A cross-validation process of 10-fold was adopted as a rule on top of the default training-test split of 70:30 to guarantee the robustness of the models and their generalizability and resistance to overfitting.

1.1.4 Compound Library Preparation

To determine possible Progesterone receptor bioactives, a phytochemical library of *Pterocarpus marsupium* of 71 chemicals was downloaded in the database of IMPPAT (Indian Medicinal Plants, Phytochemistry, and Therapeutics). Chemical structure of these phytoconstituents has been carefully curated and standardized with cheminformatics software including RDKit and Open Babel where the molecular descriptors are calculated properly and structure integrity verified. This compound library was made up (curated) and the resultant list of compounds run through predictive models based on optimized machine learning algorithms. Of the compounds that were predicted as active, priority was given to further in silico and evaluation, molecular docking and molecular dynamics to determine binding affinity, stability of the binding interaction and specificity to Progesterone receptor.

1.2 *Network Pharmacology*

Network pharmacology is a novel, complex behaviour of studying the interactions between drugs and diseases. In this paper, the analysis of bioactive compounds using state-of-the-art network pharmacology tools, i.e., STITCH and Swiss Target Prediction was undertaken on *Naringetol* in the context of breast cancer. Those were the tools used to identify possible therapeutic targets of *Naringetol*. The screening of targets and the analysis was also performed to assess the therapeutic potential based on some available resources including DisGeNET. Moreover, to consider the molecular properties of *Naringetol*, such tools as ChemDraw, PyMOL, and SwissADME were used. Cytoscape and STRING programs assisted in the network analysis of the role that Progesterone receptor plays in breast cancer pathways, allowing a deeper insight in criminal evolution of *Naringetol* on cancer processes. In silico results indicated that *Naringetol* might be used to target key breast cancer pathways, making it an attractive possibility to select it to be investigated as an anticancer medicine (29-31).

1.3 *Ramachandran States Statistics*

The Progesterone receptor (PR) protein requires a stable (structurally intact) protein to be biologically functional. The structural quality of the PR was herein assessed by calculating of Ramachandran analysis, which was carried out with the use of a program (PROCHECK) that was offered under the European Bioinformatics (EBI). Steric quality of the protein structure is also reflected due in the Ramachandran plot by calculation of dihedral angles thus evaluating to be the most suitable conformational stability of the given protein. The analysis showed the places in which the structure of the protein might hold stability, and also the places in which the deviations were probable. There were also G-factors calculated that talk more about overall stability of the protein. Bond length analysis and visual characterization of bond distributions were also structural tests and they helped to endorse the structural integrity of PR. All these studies established the structural stability of PR and this aspect indicates its ability to carry out its biological roles effectively (29-31).

1.4 *Molecular docking analysis*

Molecular docking refers to an essential algorithm of computation to investigate the interaction involved between ligand-target proteins. This study involves the docking simulations to determine the modes of binding that a number of ligands with Progesterone receptor (PDB ID: 3ZR7) with a view to understanding the modes of bonding among the compounds. It started by taking away the water molecule structure in the protein and replacing it with polar atoms so that the right ligand binding process can be effectively undertaken. Grids of docking sites on the protein were prepared and docking simulation of the geometry using AutoDock Vina were performed. The computational study of structure-based interaction between the ligands and the active site of PR was undertaken in detail to establish the therapeutic possessions of the ligands. This molecular docking study was fundamental in obtaining information on how each ligand would affect the binding capacity of receptor and it could form good data in evaluating available therapeutic strategies against PR (29-34).

1.5 *Molecular Dynamics analysis*

The molecular dynamics (MD) simulations are potent methods employed to examine the time-reliant relations between ligands and proteins. MD simulations in the present paper were carried out with the help of Desmond to investigate the dynamics of Progesterone receptor-ligand complex. The simulated system was set up so as to match physiological conditions mimicking the addition of water molecules and ions such that the system is charge neutral. The behavior of the system was studied at different temperature and pressure with different simulation time to check its ability to respond and flexibility. Important parameters Root Mean Square Deviation (RMSD) and Root Mean Square Fluctuation (RMSF) were determined in order to measure the dynamic nature and stability of the protein-ligand complex. The simulations have been shown to convey important data on the possible therapeutic effectiveness of the PR-ligand interaction which was used to ascertain the stability and behaviour of the compound in a biological environment (29-34).

1.6 *ADMET Analysis*

ADMET (Absorption, Distribution, Metabolism, Excretion, and Toxicity) analysis plays a key role in drug development because it can be used to determine forthcoming pharmacokinetics, and toxicity profile of potential treatment products. Within the present research, ADMETlab 3.0 was considered to screen the ADMET properties of the compounds in question. such a tool was used to establish predictions on vital pharmacokinetic phenomenon like intestinal absorption, blood-brain barrier permeability, interactions with cytochrome P450 enzymes, and possible toxicities. Machine learning algorithms and pharmacokinetic databases enabled ADMETlab 3.0 to produce comprehensive reports of the pharmacokinetic and safety profiles of the compounds that are critical requirements during the early drug discovery phase. This was a useful analysis in measuring drug-likeness and safety of potential therapeutic agents and aiding in the development of further optimization(29-34).

1.7 *Pharmacokinetic Simulation*

The simulated pharmacokinetics of the *Naringetol* was measured on the simulated model of a rat and an East Asian female human in PK-Sim Version 11.1 (Open Systems Pharmacology, Bayer). In the rat model, the weight allocated was 230 grams. In case of the human model, the body weight used was 59.42 kg and the healthy female with an age of 50 years had a BMI of 20.98 and was an East Asian. The anatomical, physiological and the protein expression parameters were assumed with the default values presented with the PK-Sim software. The simulation received the physico-chemical characteristic of *Naringetol* as shown below, a molecular weight (M.W.) of 272.07, a lipophilicity of 2.6 log units, and a fraction unbound of 0.07. The administration of the protocol was subjected to both models with a dose of 1mg/kg but administered orally and Intravenously (I.V.). The oral formulation was taken to be a dissolved solution. The simulation of

pharmacokinetics was done within the 24hour period in blood plasma (peripheral vein), applying the standardized PK-Sim equations of cell permeability estimation. In the case of human female model, the simulation was scaled out to represent a population of 100 human individuals the ages of which varied by 35-81 years and body weight by 36-85 kg. The rest of the physiological parameters were maintained constant to those of the actual model to achieve a validity of the extrapolation.

1.8 *Density Functional Theory*

Density Functional Theory (DFT) is method of quantum mechanics that is of consequence in regards to the electronic properties of molecules which are relevant in as far as understanding of any molecule in the aspect of reactivity and stability are concerned. DFT was employed to calculate in this work the electronic properties of *Naringetol*. Reviewing the molecular structure of *Naringetol* as it is found at PubChem, the connectivity of this substance is verified. The Spartan 14 software made the molecular energy theoretically optimized, yet the HoMO and LUMO energies were determined by GaussView 6.0.16. The estimate of the energetic distance HOMO/LUMO was discussed to be one of the indications of the reactivity and the stability of the compound. The discussion of the results of the analysis showed that a compound like *Naringetol* exhibited energy stability that was rather low, hence it provided an indication of how we can further increase the energy stability of such compounds in order to make improvements to the therapeutic potential of *Naringetol* (29-34).

1.9 *Naringetol-SLNs Formulation*

An effective system of drug delivery is the solid lipid nanoparticles (SLNs) which has greater stability and bioavailability. In the present work, *Naringetol* was added to SLNs by the application of ultrasonic dispersion and high-speed mixing. Cetyl palmitate was dissolved on the ether and the mixture was heated until a homogenous lipid complex was obtained. The mixture was then cooled down and *Naringetol* added to it, followed by ultrasonication to obtained a microemulsion. The formulation was stabilized by polysorbate-80 and sodium deoxycholate and gave a clear and stable solution. The concentrate was purified via ultracentrifugation at 10 000 rpm. Encapsulation efficiency and drug loading capacity were determined according to the standard equations. The results indicated that *Naringetol*-loaded SLNs were a good carrier medium that could increase the therapeutic property of the compound (35-37)**.**

1.10 *In* vitro Drug Release of *Naringetol*- SLNs

The dialysis bag diffusion method was imagined in the in vitro investigation of the release profile of *Naringetol*, presented by SLNs. The dialysis bags having a molecular weight cutoff of 3500 Da were loaded with *Naringetol*-loaded SLNs and incubated in release buffers of various pH (acetate buffer, pH 5.0 and phosphate buffer, pH 7.7) at 37°C. To observe the release of *Naringetol* over time, it was the High-Performance Liquid Chromatography (HPLC) that was used. The release profile was very helpful about the sustained release kinetics of the drug which was within the range of speculation that the SLNs would release *Naringetol* in a controlled and prolonged way and thus, found as useful in long term therapeutics.

1.11 *Kinetics of SLNs-Encapsulated Naringetol Release*

Naringetol release kinetics of which numerous mathematical models were applied (such as Zero Order, First Order, Higuchi, Korsmeyer-Peppas, and Hixson-Crowell) were analyzed. Those models were used with the released data to determine the release mechanism and rate of drugs released out of the SLNs. The findings were used in defining the process of the release and gave an insight to the mechanism through which *Naringetol* enters the body normally. The release kinetics of the SLNs should be analysed so that the formulation of the SLNs can be optimised such that the release of the drug is in a controlled manner and this allows the enhancement of the treatment of a disease through the treatment regime of a longer duration.

1.12 *Stability of SLNs-Encapsulated Naringetol*

1.19 The thermodynamic stability of the *Naringetol*-loaded SLNs was investigated under different physiological conditions with an aim of establishing the capacity of the particles to retain structural integrity. The formation of SLNs was carried out in BSA, acetate, and phosphate buffers (pH 5.0 and 7.7) and NaCl solution followed by an incubation process at 35°C. The maximum absorbance (lambda max) was observed on UV-visible spectroscopy overtime. The results meant that despite the morphology and stability of the SLNs in diverse conditions, the SLNs stored and used on a long-term basis. The experiment indicated *Naringetol* could be effectively encapsulated via the SLNs procedure exercising minimal impact on stability and integrity.

1.13 *LC-MS Characterization of SLNs-Encapsulated Naringetol*

1.21 Liquid Chromatography-Mass Spectrometry (LC-MS) was also used to describe the stability, as well as the integrity of *Naringetol* within SLNs. LC-MS analysis reported that *Naringetol* was not lost or degraded thus it was able to be incorporated into the SLNs. The spectroscopic results provided another evidence regarding the fortitude of the compound and can be employed to defend the fact that the *Naringetol*-loaded SLNs can serve as drug-delivery vehicle.

1.14 Particle Size Analysis *of SLNs-Encapsulated Naringetol*

To investigate the Andrographolide-loaded SLNs, dynamic light scattering (DLS) is employed to determine the particle size and size distribution. The size distribution histogram reveals a monomodal distribution, with a peak intensity at approximately 50 nm, indicating high homogeneity and low polydispersity. This narrow distribution confirms the absence of aggregation and demonstrates the consistency in nanoparticle size, essential for reproducible drug release and pharmacokinetic performance. Zeta potential analysis is performed to evaluate the surface charge of the SLNs. A moderate negative surface potential of -10 mV is observed, indicating the presence of negatively charged functional groups, likely from lipid components or stabilizers. This negative charge provides sufficient electrostatic repulsion to prevent aggregation, ensuring colloidal stability. The narrow and symmetric bimodal distribution of zeta potential further supports uniform surface charge distribution.

The combination of optimal particle size (<100 nm) and moderate negative surface charge offers favorable conditions

for enhanced cellular uptake, prolonged circulation time, and improved bioavailability, making Andrographolide-loaded SLNs a promising delivery system for therapeutic applications.

1.15 *FTIR Characterization of SLNs-Encapsulated Naringetol*

The effect of molecular interaction between *Naringetol* and the SLNs was characterized using Fourier Transform Infrared Spectroscopy (FTIR). The FTIR analysis covered the range of 400-4000 cm^{-1} by use of a Shimadzu IR Tracer-100. The functional group involved in encapsulation process was found based on the information given in the spectra and also it was established whether any kind of interaction between *Naringetol* and the lipid components of the SLNs was happening or not. The data revealed has shown *Naringetol* or overall product, keeping structural integrity of the original drug undergoing the encapsulation remained consistent and was also at a molecular level compatible.

1.16 *SLNs Loaded with Naringetol Analysis by FE-SEM*

Morphology and size distribution of *Naringetol*-loaded SLNs was investigated by means of Field Emission Scanning Electron Microscopy (FE-SEM). Frozen-dried materials were reconstituted with the help of distilled water, and FE-SEM examination was carried out to determine their morphology. The analysis indicated that the SLNs are homogenous and stable, an aspect that is very vital in their use in controlled drug delivery systems. The research established that the SLNs could be used as a prospective vehicle of sustained-release formulations to explore a greater therapeutic response of *Naringetol*.

1.17 *MTT Assay*

MTT analysis was done to calculate and determine the cytotoxicity of *Naringetol*-loaded SLNs in the MCF-7 cells that were used as breast cancer cells. The cells were propagated in the DMEM/FBS media which had penicillin and streptomycin antibiotic, the wanted doses of the *Naringetol*-loaded SLNs were added to the cells and incubated overnight at 37C. The reagent (MTT) was added onto incubation and the 570 nm absorbance was used as a tool to measure the cell viability. These results demonstrated that *Naringetol*-loaded SLNs were biocompatible and they possessed superior anticancer effects, and they could be used as a future anticancer therapeutic product (29, 36).

1.18 *Cytotoxicity Assay*

*Preparation of stock solutions*1.31 mg of Naringetol SLNs were dissolved in 1 mL of Dimethyl Sulfoxide (DMSO) to create a stock solution with a concentration of 10 mg/mL. After that, this stock solution was kept at -80°C. To guarantee sterility, the stock solution was diluted in a complete medium and then passed through a sterile 0.22 um filter to create a working solution with a concentration of 1 mg/mL. Carboplatin (CBP), a common medication, was also diluted in a full culture medium to achieve Naringetol SLNs concentrations of 2.5, 5, 10, 15, 20, 25, and 50 µg/mL.

1.19 *Cytotoxicity assay of Naringetol SLNs*

Cell cytotoxicity was evaluated using the MTT conversion test. In a 96-well plate, MCF7 cells were added at a density of 5x104 cells/ml. The cells were treated with *Naringetol SLNs* at different doses, ranging from 2.5 µg /ml to 50 µg/ml. Following treatment, each well received 20 µL of a 5 mg/mL MTT solution, which was then incubated for four hours. The formazan crystals were then dissolved in each well by adding 100 µL of DMSO. The Multi-scanGo Thermo Fischer Scientific ELISA plate reader was used to measure the absorbance at 570 nm. An Excel worksheet from Microsoft Office was used to determine the IC_{50} value(12, 30, 31)

1.20 *Apoptosis analysis*

The FITC Annexin V/Dead Cell Apoptosis Kit (Invitrogen-Naringetol SLNs) was used to conduct the apoptosis experiment. The manufacturer's instructions were adhered to. These stained cells were examined using flow cytometry at emission wavelengths of 530 and greater than 575 nm. In this test, the apoptosis assay was conducted using the IC_{50} values of CBP, Naringetol SLNs (14, 28).

1.21 *In vivo Breast Cancer Activity*

1.21.1 Subcutaneous xenograft establishment

A 1-week acclimatization of the 6 to 8 weeks female nude mice in an SPF barrier facility was done. The log-phase MCF7 cells were collected using 0.25% trypsin, washed twice using a sterile PBS and resuscitated at 5x106 cells/100 mL. A syringe (1 mL) was loaded with 100 mL of the suspension; alcohol swab was used to disinfect the right axillary dorsal skin. The needle was injected subcutaneously and gradually(32, 33). Following the withdrawal, the samples were gently scraped during 3 s to avoid any leakage. Day of inoculation was considered to be Day 0; nodules could be palpated in 5-7 days with a take rate greater than 95%.

1.21.2 Tumor volume measurement

Measurement of tumors began on Day 15, after which the tumors were measured weekly. While the longest diameter (L) and the perpendicular shortest diameter (W) were measured using electronic digital calipers. The volume was estimated using the normal formula: V = 0.5 LW2. Measurements were done by the same operator in the period 9:00 to 11:00 a.m. up to Day 43.

1.21.3 Tumor mass determination

At the endpoint, the mice were euthanized using CO_2. Sterilization of the tumor region was done using 75% ethanol, skin incision was done with ophthalmic scissors and the whole tumor bluntly dissected. Blood vessels, fascia and necrotic tissue were excised and the tumor rinsed in ice-cold PBS, blotted on filter paper, and weighed on a 0.1 mg precision scale balance (Sartorius). Error was checked to be less than 0.2 mg every day.

1.3 Results and Discussion

1.3.1 Comparison of Machine Learning Models

The performance of machine learning algorithms coupled with the classifier to determine the outcome of the bioactivity of compounds targeting Progesterone receptor was tested using some standard metrics of evaluation such as accuracy, Kappa statistic, Mean Absolute Error (MAE), Root Mean Squared Error (RMSE), Relative Absolute Error (RAE), and Root Relative Squared Error (RRSE). Random Forest topped all the tested models in its predictive accuracy of 78.12%, a strong Kappa value of 0.5361, and the lowest errors with the mean absolute error rate of 0.2004 and root mean square error rate of 0.3204 representing brilliance in accuracy and insignificance of error. The second algorithm Decision Tree resulted in an accuracy of 75.85% and a Kappa of 0.4716 and the third model K-Star attained an accuracy of 75.19% and Kappa of 0.4679. Compared to them, other models, including Naive Bayes, Multilayer Perceptron, Logistic Regression, and Sequential Minimal Optimization (SMO) possessed

lower accuracies of 69.91%, 75.19%, 71.89%, and 71.72%, respectively; their Kappa statistics remained lower, whereas their error rates were higher, which implies that they turned out to be less robust in their classification tasks. For model generalizability, the Random Forest classifier was further validated on the test set, achieving an accuracy of 79.98%, a Kappa statistic of 0.6414, and corresponding MAE and RMSE values of 0.1825 and 0.3107, respectively. These results confirm the reliability and robustness of the Random Forest model, making it an effective tool for accurately predicting the bioactivity against Progesterone receptor, with significant potential for application in drug discovery **Figure 1-4** and **Table 1-4**.

Table 1 Performance comparison of various machine learning models based on key evaluation metrics: accuracy, kappa, mean absolute error (MAE), root mean square error (RMSE), relative absolute error (RAE), and root relative squared error (RRS).

Model	Accuracy (%)	Kappa	MAE	RMSE	RAE (%)	RRS (%)
Random Forest (RF)	79.06	0.5333	0.1881	0.3068	60.26	77.72
Kstar	75.19	0.4679	0.1663	0.3892	53.28	98.60
Decision Tree	75.19	0.4563	0.1828	0.3817	58.57	96.68
IBK (k-NN)	75.85	0.4716	0.1855	0.3727	59.44	94.42
Multi-Layer Perceptron	71.89	0.3561	0.2524	0.3583	80.88	90.76
Naive Bayes	71.89	0.4027	0.1881	0.4323	60.28	109.51
Logistics	71.72	0.3402	0.2876	0.3735	92.17	94.60
SMO	69.91	0.3278	0.2399	0.3866	76.86	97.93

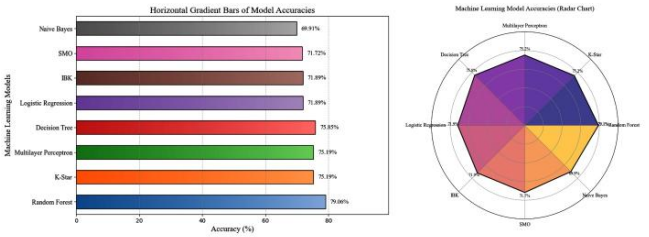

Fig. 1 The figure presents model accuracy comparisons using two chart types: a vertical bar chart (left) showing the accuracies of various machine learning models, and a radar chart (right) for a more detailed view.

Table 2 Performance metrics for the classification model, including accuracy, kappa, mean absolute error (MAE), root mean squared error (RMSE), total instances, and correctly/incorrectly classified instances.

Metric	Value
Accuracy	78.12%
Kappa	0.5361
Mean Absolute Error (MAE)	0.2004
Root Mean Squared Error (RMSE)	0.3204
Total Instances	521
Correctly Classified Instances	407 (78.12%)
Incorrectly Classified Instances	114 (21.88%)

Table 3 A Confusion matrix showing the classification of activity levels. The rows represent the predicted activity levels (Moderately Active, Active, Least Active), and the columns represent the actual activity levels.

	a (Moderately Active)	b (Active)	c (Least Active)
a (Moderately Active)	136	55	0
b (Active)	53	271	0
c (Least Active)	2	4	0

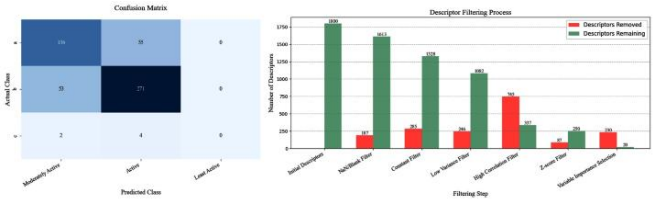

Fig. 2 Left: Confusion matrix showing the performance of the classification model for different activity classes. Right: Stacked area chart illustrating the descriptor filtering process with cumulative removal of descriptors across various filtering steps.

Table 4 Descriptor filtering process for feature selection, showing the number of descriptors removed and remaining at each filter step, including NaN/Blank, Constant, Low Variance, High Correlation, Z-score, and Variable Importance filters.

Filter Step	Descriptors Removed	Descriptors Remaining
Initial Descriptors	-	1800
NaN / Blank Filter	187	1613
Constant Filter	285	1328
Low Variance Filter	246	1082
High Correlation Filter	745	337
Z-score Filter	87	250
Variable Importance	230	20

Fig. 3 Two correlation heatmaps showcasing the relationships between various variables, with color gradients representing correlation strength. Positive correlations are shown in red, while negative correlations are in blue.

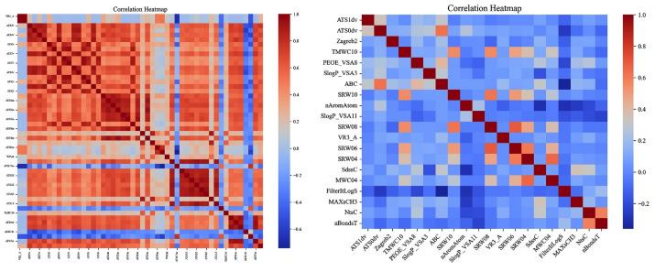

Fig. 4 Two visualizations comparing model performance metrics: (left) a heatmap of various model performance metrics (Accuracy, RMSE, MAE, RAE, and RRSE) for different models, and (right) a radar chart with normalized values for each metric.

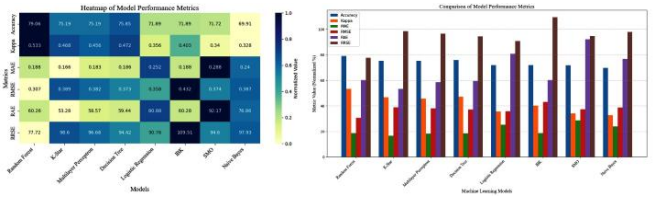

Prediction of Progesterone receptor Activity for Rubia cordifolia Constituents

The optimized Random Forest model was applied to screen a phytochemical library derived from Pterocarpus marsupium, comprising 71 compounds, to identify potential inhibitors of GLO1. Among the compounds evaluated, the following were predicted as "active" based on their molecular descriptors, indicating their potential as therapeutic candidates for targeting Progesterone receptor: Naringetol and Propterol-b. To validate these predictions, further computational analyses, including molecular docking and molecular dynamics simulations, are necessary to assess their binding affinity, interaction stability, and specificity towards the Progesterone receptor active site. Such analyses will guide the

prioritization of these compounds for subsequent experimental validation, further supporting their role in drug development.

3.2 *Network Pharmacology*

Network analysis of the major proteins showed the presence of outstanding variations to the degree of the measures of centrality of their networks that showed that they could be participating in vital cellular pathways. The top proteins in terms of degree were PDX-1-REP that scored 57 and PGR that had a score of 57. It also had a high radiality, which emphasized its communication in linking different pathways and regulation of cellular communication. Other proteins that revealed high connectivity were MAPK and BRCA1 (56 and 52, respectively), as well as their betweenness values indicating that these two proteins are among the central ones in cancer-related signaling pathways. Conversely, proteins with the degree of 40 such as HRAS showed fewer interactions and yet served as critical signals as illustrated in the betweenness indicator and closeness indicator. The analysis also pointed at the crucial importance of the proteins, namely PARP, BRD4, and TP53, with the degree of 49, which is identical and, therefore, means that they equally affect the network. Rather interestingly, the tumor suppressor gene, TP53 had high scores on eccentricity and stress indicating that it is a key gene involved in determining the pattern of cellular response to stress and damage. With regard to therapeutic targets, the proteins of the network, namely BRCA1, PARP, and AKT1, indicated high potential in cancer therapy. It is found that these proteins are the potential intervention points in the case of natural as well as synthetic drug therapies, since it is the protein that directly relates to the cellular survival and apoptosis process. The differences in level and position of these proteins in the network indicate a possible role of these proteins as targets of new combinations of drugs in trying to circumvent resistance pathways in cancer therapy **Figure 5** and **Table 5**.

Table 5 Network centrality metrics for various proteins, including degree, betweenness, closeness, eccentricity, eigenvector, radiality, and stress. These metrics describe the importance and connectivity of proteins in a given network.

Protein	Degree	Betweenness	Closeness	Eccentricity	Eigen-Vector	Radiality	Stress
PGR	57	13.733232	0.019608	0.5	0.160728	1.959184	354
MAPK	56	15.2289	0.02	0.5	0.163266	1.979592	390
BRCA1	52	14.77828	0.02	0.5	0.163309	1.979592	386
KEAP-1	51	11.29542	0.018519	0.5	0.150854	1.897959	296
CDKN2A	49	15.2289	0.02	0.5	0.163266	1.979592	390
PARP	49	16.63513	0.020408	1	0.165839	2	424
BRD4	49	16.63513	0.020408	1	0.165839	2	424
TP53	49	16.63513	0.020408	1	0.165839	2	424
KRAS	48	15.50591	0.02	0.5	0.163117	1.979592	394
ERBB2	48	12.87538	0.019231	0.5	0.157375	1.938776	338
SMAD4	47	14.01023	0.019608	0.5	0.160579	1.959184	358
BRCA2	46	12.02779	0.018868	0.5	0.153865	1.918367	318
CDK4	46	13.3993	0.018868	0.5	0.153385	1.918367	336
TERT	46	12.00583	0.018868	0.5	0.154393	1.918367	316
ESR1	45	10.4478	0.018868	0.5	0.155591	1.918367	284
TTR	45	7.331822	0.015625	0.5	0.115028	1.693878	190
MYC	45	10.26242	0.018868	0.5	0.155801	1.918367	280
BRAF	45	11.34765	0.018519	0.5	0.151577	1.897959	286
MSH2	44	9.360374	0.017857	0.5	0.144505	1.857143	250
BCL2	44	6.37175	0.017241	0.5	0.139947	1.816327	178
CCND1	44	8.429123	0.018519	0.5	0.153277	1.897959	242
NRAS	44	7.871037	0.018182	0.5	0.150391	1.877551	224
AKT1	43	8.296584	0.018182	0.5	0.150007	1.877551	230
STK11	43	9.722441	0.017857	0.5	0.145108	1.857143	254
MDM2	43	7.071266	0.017544	0.5	0.14369	1.836735	194
EGFR	43	8.8395	0.017857	0.5	0.145627	1.857143	238
NF1	42	7.120237	0.017241	0.5	0.13977	1.816327	196
MLH1	41	7.802155	0.017241	0.5	0.137932	1.816327	212
CDK2	41	9.704653	0.017241	0.5	0.137366	1.816327	244
HRAS	40	5.14642	0.017241	0.5	0.141465	1.816327	154
CHEK2	40	8.222605	0.016949	0.5	0.134406	1.795918	218
STAT3	40	4.469942	0.016949	0.5	0.137695	1.795918	136
CDKN1A	40	5.261295	0.016949	0.5	0.137546	1.795918	150
CDH1	40	3.963355	0.016949	0.5	0.138339	1.795918	122

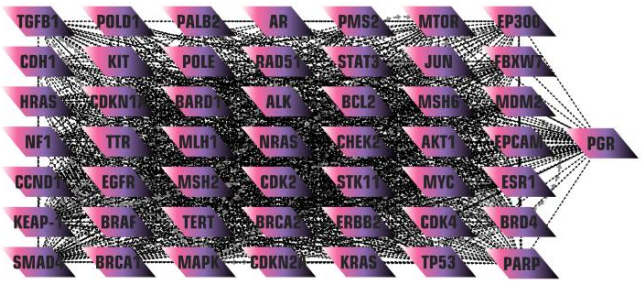

Fig. 5 Network analysis of key proteins with their connectivity metrics: Degree, Betweenness, Closeness, and Stress. Higher centrality values indicate crucial roles in cellular pathways.

3.3 *Analysis Statistics of Ramachandran Plot*

The investigations on the torsion angles (PHI and PSI) which are versus of the Ramachandran plot yield structural clues which are quite important. The 3D and the 2D plots have shown there is a significant location of torsion angle values concentrated around particular area, conveying the susceptibility of the dimensions and tendency of the residues. They see that most of the residues are found in the preferred and permitted zones of the Ramachandran plot, which indicates that the structure has been optimized well as regards to backbone geometry.

As shown on the 3D plot, it can be clear that the torsion angles are incredibly concentrated on some regions, especially on specific residues, where the manifold of occurrence can be more noticeable on particular torsion angles values. It goes in line with the resistance to folding and stability of the protein in these domains. The respective 2D contour plot

makes this observation more precise by illustrating the torsional angle density, the densest being located in the most preferred areas. The fact that the measurements made using both of these plots are consistent also contributes to the strength of such findings, so the existence of the overall correlations between the 3D and 2D plots confirms the stability and good geometry of the examined structure. There are only a few residues in the prohibited areas and this indicates that the protein structure is mainly stable with little steric collision or unpleasant torsion angles. These might be suggestive of areas of flexibility/variability which may be part of functional movements or binding of ligands. An investigation of these residues further may reveal effects of the slightest alterations of the backbone geometry on protein functionality. The Ramachandran statistics observed indicate that the protein under consideration have a normal conformational behavior, and the percentages of residues within those favored areas is exceptionally high. It is a sign of a properly organized, practically effective protein, and this corresponds to the stability of such structures and their biological activity **Figure 6**.

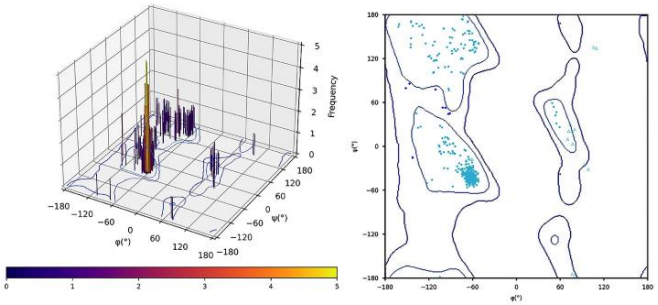

Fig. 6 3D and 2D Ramachandran plots of torsion angles (PHI and PSI) showing the distribution of residues in the favored, allowed, and disallowed regions, with frequency representation of angle distributions.

3.4. Molecular Docking Analysis

The docking of the ligands contained in this study has shown that the ligands have different affinities to the target protein. Comparing the docking score of the compounds, 74-Dihydroxyflavone had the lowest docking score of -9.3 which did not vary in both cases indicating a stable docking with the protein. Likewise, Naringetol also exhibited significant binding capacity with docking score of -12.3. Liquiritigenin and Pseudobaptigenin were also a promising advance with the scores of -9.2 and -9.1, respectively, meaning that they showed a moderate binding affinity. The substances are natural products and can form promising leads in drug discovery. Epicatechin and Isoliquiritigenin on the other hand showed a docking score of -9.0 indicating lower docking interactions than the compounds above albeit within a probable range to have any form of therapeutic uses. Compounds with a moderate potential binding score were similar such as 374-Trihydroxyflavone (-8.7), 2S-7-hydroxyflavanone (-8.5) and 4-2-hydroxy-3-4-hydroxyphenylpropylphenol (-8.3). Remarkably, the lowest affinities of all the tested compounds were confirmed by beta-Eudesmol and Ebanol (-7.9 and -7.7), respectively. This implies that their chances of a high interaction with target protein are less. The binding affinity results indicate that most of the tested flavonoid and phenolic molecules have good potential of binding to the target protein, with the highest binding affinity identified in *Naringetol*. More lab-based finding such as in vitro testing as well as structural studies are encouraged to validate the therapeutic efficacy of these chemicals. The results indicate that the number of types of molecular interactions existing between the 3ZR7_*Naringetol* complex and the 3ZR7_*Naringetol* interactions number more than one and are composed of such interactions as the hydrophobic interaction, the hydrogen bond, and the pi-stacking. The residues LEU (721A, 763A) and TYR (890A) are residues with hydrophobic interaction and the Hydrophobic interaction distance lies between 3.55 to 3.99A and hence it can be stated that there must be significant non-polar interaction between the ligand and residues. Such interactions at different sites on the dent of the protein signifies a place where the ligand can be able to bind in a well manner in relation to stable or conformation of the protein ligand complex. The H bonds that appear to be most crucial in molecular recognition and stability occur, specifically in residues ASN (719A), GLN (725A), and ARG (766A). The distance between the hydrogen bond donor and hydrogen bond acceptor are 1.94 to 2.95 Angstrom and the angled width is computed as 128.44 to 149.23. The bonds assist in the right direction and specific binding of the ligand to the protein. Notably, the protein donors in the contact, such as atoms such as [Nam] and [O3] support the creation of a mesh stability interaction, which supports the maximisation of the ligand binding. Finally, π-stacking interactions involving phenylalanine (PHE) residue (778A) and the ligand at distance 4.74 A and angle 83.03 o were also there. The increase of the overall stability and specificity in the ligand binding come off, 2482, 2483, and 2484 ligand atoms are determined to produce the 11-stacking **Figure 7**.

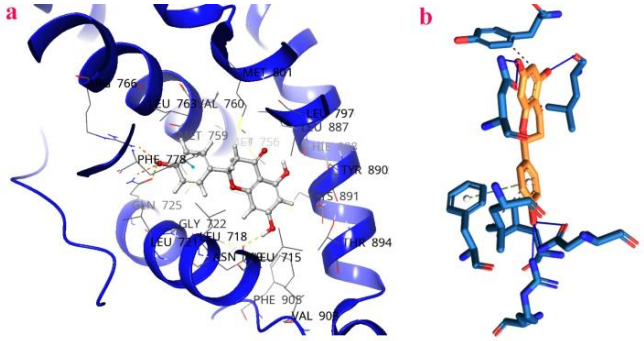

Fig. 7 A molecular interaction analysis, with the left image displaying protein-ligand binding and the right highlighting the interaction between residues and a ligand through hydrogen bonds (dashed lines).

3.5. Molecular Dynamics Measurements

3.5.1 Root Mean Square Deviation (RMSD)

The extent of RMSD is applied in defining the variation of the positions of the atoms in a protein and the ligand with respect to time during molecular dynamics (MD) run. Figure 8a gives the RMSD value of protein and protein fitted with ligand as a function of time in nanoseconds. The RMSD value of the protein is relatively stable within the standard deviation of 0.4 to 1.4 angstroms having a relatively steady plot showing that the simulation does not alter the integrity of the protein structure significantly. The ligand RMSD is a little more prominent and varies between 0.2 to 1.6 A on which it is believed that the ligand itself experiences some variant in its conformation or rearrangements as it is interacted with the protein. The low value of the RMSD of the protein implies that the protein-ligand interaction does not imply any drastic alterations to the protein structure and the ligand does not move so much in the binding pocket. But the changes of ligand RMSD show that the ligand might have varied binding poses within the simulation **Figure 8a**.

3.5.2 Root Mean Square Fluctuation (RMSF)

Fig. 8b contains the RMSF values that illustrate the variation of individual residues in the course of the simulation. The RMSF pattern of the protein indicates that certain residues had higher peaks and particularly at the loop positions and other regions having flexible secondary structures. High RMSF indicates parts of the protein which experience large conformational fluctuations or are flexible and the low RMSF values indicate structural stability. The data shows that there are parts of protein that are more flexible and this could be

related with the parts of binding area or those parts of interaction with the ligand. The ligand as well shows fluctuations though they are not very dramatic. The concentrations of RMSF of the ligand are mostly concentrated on the interactions with the protein mainly indicating the binding site residues have strong influence by exerting some force on the ligand, which affects the stability and its conformation **Figure 8b**.

3.5.3 Protein Ligand (PL) Contacts

Figure c profiles the dynamic of protein- ligand interactions over time and each line is the profile of interaction of certain residues with ligand. The result at the upper part of the figure is a total contact plot revealing changes in the number of the contacts in time. The interactions in the inset are in the format of a heatmap format of specific residues, LEU 715, ASN 719, and LEU 718 that have higher and more intense contact with the ligand. Such constant interactions indicate that these residues play a significant role in stabilizing protein-ligand complex. These results are verified by the interaction made fraction bar chart (Figure 8c and d), which shows high contact fractions within residues such as LEU 715, LEU 718 and ASN 719 but the remaining residues are less with interactions. In the chart, it is also clear that some of the residues make more contributions to the binding energy implying that the residues are key determinants of the complex stability **Figure 8c**.

1.39.4 Torsion Angles

The plot of torsion angles (as showed in Figure 8e) shows how the ligand changes during the simulation. The torsion angle graphs depict regular oscillation of the dihedral angles of the ligand, especially those that are flexible in the molecule. Such changes play a major role in the comprehension of the ligand adaptability during its binding, since the changes in torsion angles could be the cause of the best fitting with the protein binding site. These torsional changes may affect the binding energy of the complex, they are displacements of conformational motions available to the ligand, inside the binding pocket **Figure 8d**.

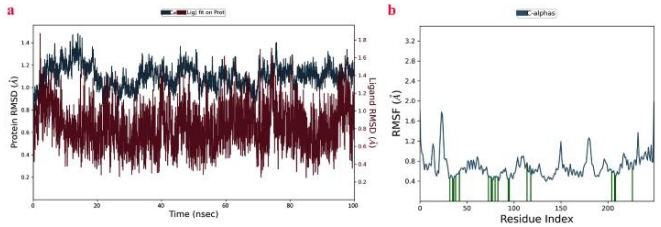

Fig. 8 a) show the RMSD of the protein and ligand, indicating the structural stability over time. b) shows the RMSF for protein residues, highlighting regions of flexibility. c) displays PL contacts over time, and d) shows the torsion angle analysis of the ligand during the simulation.

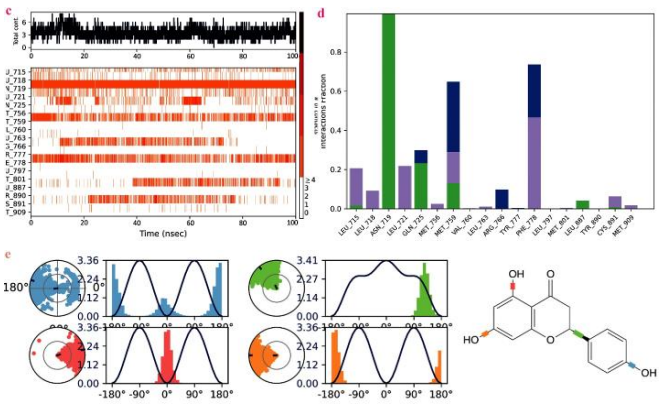

1.39.5 MMGBSA Analysis

The molecular mechanics generalized Born surface area (MMGBSA) calculations reveal the energetic contributions to ligand binding for Ligand 1. The analysis decomposes the total binding free energy (ΔTOTAL = -59.00 ± 0.69 kcal/mol) into distinct thermodynamic components. Van der Waals interactions (ΔVDWAALS = -63.28 ± 0.68 kcal/mol) provide the most favorable contribution to binding, indicating strong hydrophobic contacts between the ligand and protein binding site. Electrostatic interactions (ΔEEL = -25.13 ± 0.10 kcal/mol) also contribute favorable to binding affinity. However, these favorable interactions are partially offset by the polar solvation penalty (ΔEGB = +37.53 ± 0.43 kcal/mol), which represents the energetic cost of desolvating polar groups upon binding. The nonpolar surface area term (ΔESURF = -10.62 ± 2.77 kcal/mol) provides a modest favorable contribution. Overall, the negative total binding free energy indicates thermodynamically favorable binding, with van der Waals interactions being the primary driving force for complex formation.

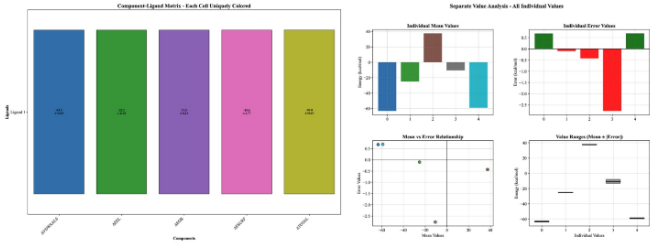

Fig. 8f Component-Naringetol Matrix displays uniquely colored cell data across five components (ALCOHOL, JUICE, CREAM, CHEESE, PIZZA), while separate value analysis shows individual means, errors, relationships, and ranges.

3.6. *ADMET Analysis*

The physicochemical and toxicity profile of *Naringetol* is presented in the figures, showcasing various molecular properties and potential risks associated with its use. Figure (a) provides an overview of *Naringetol*'s key physicochemical parameters, including molecular weight (272.26 Da), logP (2.51), hydrogen bond acceptors (5), hydrogen bond donors (3), rotatable bonds (1), and the polar surface area (TPSA) of 86.99 Å^2. These values indicate moderate lipophilicity and favorable drug-like properties, suggesting that *Naringetol* may have suitable bioavailability for drug formulation.

Figure (b) evaluates the compound's ADMET (absorption, distribution, metabolism, excretion, and toxicity) properties, with a focus on its safety score (1216.3) and categorization into the medium risk zone based on established thresholds. The risk classification includes low potential for mutagenicity, carcinogenicity, hepatotoxicity, and skin sensitization, but highlights potential concerns regarding cytotoxicity.

Figure (c) provides a visual representation of *Naringetol*'s position on the drug-like properties plot, with respect to TPSA and other key parameters. *Naringetol* falls within the medium risk zone, suggesting that while it has promising physicochemical properties, further safety evaluations, particularly concerning cytotoxicity, may be necessary for clinical applications **Figure 9**.

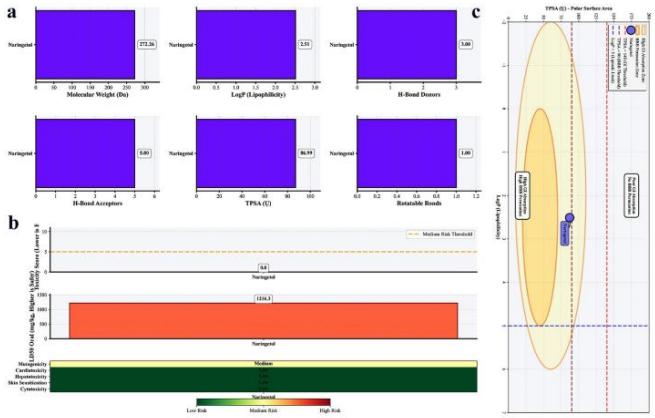

Fig. 9 Physicochemical and toxicity profiling of Naringetol. (a) Molecular properties including molecular weight, logP, hydrogen bond donors/acceptors, rotatable bonds, and TPSA. (b) ADMET safety score with risk classification. (c) Drug-like properties analysis plot showing Naringetol's medium risk classification.

3.7. *Pharmacokinetic Simulation*

Pharmacokinetic parameters of the rats, female subjects, and the total of a 100 female group were simulated for the intravenous (IV) and oral administration of *Naringetol* at 1 mg/Kg dosage. The findings reveal significant variations in the routes of the drug in absorption, distribution and elimination between the two modes of drug administration. In the case of rats, the AUC∞ with the IV administration (10843.73 *µg*min/ml) was far much higher than in the case of oral administration (8560.07 820.37 *µg*min/ml), which means that the absorption and systemic exposure was more efficient in the case of IV administration. Likewise, in the case of the female individuals, it was found that the administration through IV is better as the AUC is high (2626.56 *µg*min/ml) when compared to the one obtained by oral administration (2541.72 *µg*min/ml). The same trend occurred in the 100 group of women where IV administration demonstrated an AUC∞ of 4307.11 *µg*min/ml as compared to 4030.75 *µg*min/ml with the oral administration. The half-life of *Naringetol* was interestingly higher in rat model than in human model, but the prediction shows elevated median half-life in the population 100 individuals. To understand this projection, *Naringetol*'s half-life was mapped with body weight of the individuals (figure 2) which revealed that the body weight has positively influenced the half-life. This must be due to higher lipophilicity of the compound facilitated the retention in physiology with higher fat and muscle contents. This insists that the dosage of *Naringetol* has to be determined based on the body weight and fat content **Figure 10** and **Table 6**.

Table 6 The pharmacokinetic parameters (AUC∞, AUCtEnd, Cmax, CtEnd, total body clearance/F, MRT, t_max, half-life, Vd, and Vss) for rats, female individuals, and 100 females following IV and oral administration.

Parameters	Rats		Female Individual		100 females	
	IV	Oral	IV	Oral	IV	Oral
AUC_{∞} [µg*min/ml]	10843.73	8560.08	2626.56	2541.72	4307.11	4030.75
AUC_{tEnd} [µg*min/ml]	746.71	706.91	398.74	399.78	285.28	287.47
C_{max} [µg/ml]	1.87	0.64	3.15	1.28	2.87	1.14
C_{tEnd} [µg/ml]	0.45	0.44	0.18	0.18	0.13	0.13
Total body clearance/F [ml/min/kg]	0.09	0.12	0.38	0.39	0.28	0.30
MRT [h]	373.35	294.50	200.69	192.27	522.07	484.19
t_max [h]	0.05	1.40	0.05	0.55	0.05	0.53
Half-Life [h]	260.7	205.1	146.30	140.3	369.24	343.0
Vd (plasma)/F [ml/kg]	3 2081.29	5 2074.54	4821.44	8 4780.82	7361.97	8 7312.27
Vss (plasma)/F [ml/kg]	2065.81	2064.21	4584.38	4538.75	7180.55	7118.14

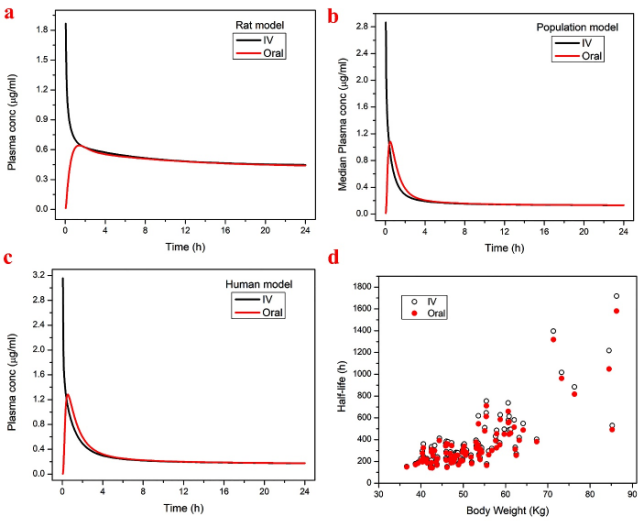

Fig. 10 The figure displays plasma concentration-time curves for the rat (a), human (b), and population (c) models following intravenous (IV) and oral administration. Data are presented for 24 hours (d), Scatter plot illustrating the relationship between body weight (kg) and half-life (h) for both intravenous (IV) and oral drug administration. IV is represented by open circles, while oral administration is indicated by red circles.

Limitations

In this study, the pharmacokinetics of *Naringetol* were predicted using both rat and human models. However, conducting an in vivo study on rats to further optimize the physiology of the organism would provide more accurate allotropic extrapolation to human models. Such a study would enhance the precision of the pharmacokinetic predictions and offer valuable insights into the translational aspects of the drug. Despite the potential advantages of direct in vivo experimentation, ethical concerns have led us to model the rat physiology using PK-Sim software. In this simulation, the rat model was assigned a body weight of 230 g, which was randomly selected for the purpose of this study. This modeling approach enables us to conduct further research on rats in the future, should the study progress to experimental validation, allowing for a more comprehensive understanding of the pharmacokinetic properties of *Naringetol*.

3.8. *Density Functional Theory*

The above figure shows Lowest Unoccupied Molecular Orbital (LUMO) and Highest Occupied Molecular Orbital (HOMO) of *Naringetol*. The HOMO was computed as -0.33387 that shows the electron donating property of the molecule. The component of the LUMO value at -0.19741 is the ability of the molecule to receive electrons. The analysis of electronic transitions in the molecule is observed to have an energy gap (DE) between two frontier molecular orbitals (HOMO and LUMO) 3.713 eV. This value shows also the capacity of the molecule to display effective charge transfer in molecular interactions. The high ΔE normally means high stability and the relatively medium ΔE on *Naringetol* makes it prone to reacting in electron transfer reactions. The spatial arrangement of the HOMO and LUMO orbitals can be seen to display a large amount of overlap of electrons in the aromatic parts,

and strong participation of oxygen atoms within the conjugation. This may increase the binding of the molecule to biological receptors particularly in system exclusive to electronic-rich substances. Also, the orbital forms and energies give information about the conduct of the molecule under a pharmacological aspect that may induce a certain binding on a specific receptor or enzyme. Such results are significant to the properties of the molecule *Naringetol*, and its potential reactivity with other molecules in a variety of biological domains. It comes out that the 27.19 kcal/mol calculated 2E supports the potential of *Naringetol* as a potentially effective drug design because electron transfer can contribute to their mechanism of action **Figure 11**.

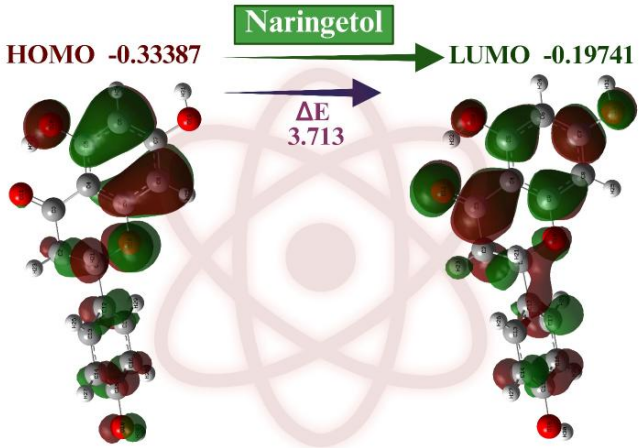

Fig. 11 The molecular orbitals of Naringetol, showing the HOMO (-0.33387), LUMO (-0.19741), and the energy gap (ΔE = 3.713 eV) between them, providing insights into its electron-donating and accepting properties.

3.9. *Naringetol-encapsulated SLNs*

The encapsulation efficiency of this formulation has been determined as 94.00 % which is a high percentage of success in the encapsulation process. The high percent encapsulation indicates that a percentage of the active compound was efficiently added in the carrier system, something that is essential in the achievement of the therapeutic effect. Efficient encapsulation is usually connected with a higher stability and a controlled release of the active ingredient which helps to increase the effectiveness of the formulation during the years. Conversely the loading capacity of the formulation was assessed as 9.26% which is not high. On the one hand, the loading capacity indicates the content of the active ingredient that can be added to the carrier, but the proportion is not high enough, so there is a possibility to optimize the formulation procedure. The loading capacity may need to be increased; this could possible increase the carrying capability of the formulation with higher dosing of the active, and this may be advantageous in some therapeutic applications. In general, the high encapsulation efficiency and moderate loading capacity represent the high potential of further optimization and development of the formulation. The research in future can be directed towards increasing the loading capacity and maintain the encapsulation efficiency and this would provide a superior drug delivery system **Figure 12**.

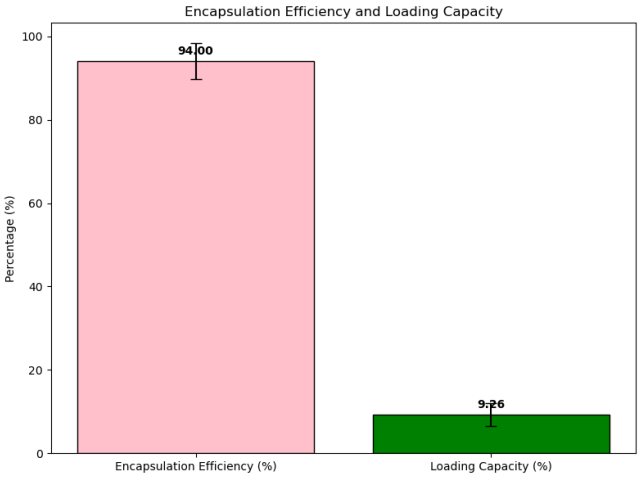

Fig. 12 The bar chart shows the encapsulation efficiency (94.00%) and loading capacity (9.26%) of the formulation, with error bars indicating variability in measurements.

3.10. *In vitro release of Naringetol from SLNs*

In vitro release of *Naringetol* loaded in solid lipid nanoparticle (SLN) was measured at two differing pH; pH 5.0 (acetate buffer) and pH 7.7 (phosphate buffer). When the experiment was performed at 5 hours, a considerably lower release percentage was also noted at pH 5.0 with the *Naringetol* liberated being only about 20 percent. In comparison, it was released with a lot higher percentage of around 60% in the conditions of pH 7.7. At 75 hours, the tendency remained the same, with pH 7.7 releases being significantly higher and approximately 85 percent, compared to those of pH 5.0, which were lower, and approximated 40 percent. This proves that when *Naringetol* is released at more neutral pH of 7.7, it is released faster than at a more acidic pH of 5.0. The changes in the *Naringetol* molecule solubility and stability at various pH levels could be blamed on this condition. The low rate of release over the period in phosphate buffer observed at the both time point implies that SLNs showing sustained release profile may be a good applicant in drug delivery system and sustained effect is expected especially in physiological conditions where the pH is towards the neutral side **Figure 13**.

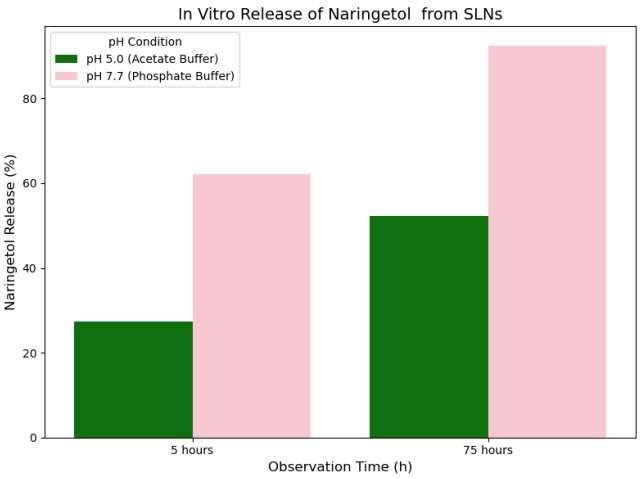

Fig. 13 The figure illustrates the in vitro release of Naringetol from SLNs under different pH conditions: pH 5.0 (acetate buffer) and pH 7.7 (phosphate buffer) at 5 and 75 hours.

3.11. *Drug release kinetics of Naringetol - encapsulated SLNs*

Drug release kinetics of *Naringetol* entrapped Solid Lipid Nanoparticles (SLNs) was investigated using the different kinetic models at pH 5.0 and 7.7 such as Zero-order, First-order,

Higuchi, Korsmeyer-Peppas and Hixson-Crowell models. The computed r^2 values in all the models of the kinetics were consistent between the two pH values. However, the Higuchi model showed the highest r^2 value of 0.9811 at PH of 7.7 implying that at this pH, the drugs release obeys the process of diffusion. In the other models, the values of r^2 did not vary with pH and were maintained at 0.920 in both 5.0 and 7.7, which shows that change in pH did not affect release kinetics in these two models. This regularly occurring tendency suggests that *Naringetol*-loaded SLNs possessed steady release characteristics, irrespective of the availability of the neighboring pH levels. These results indicate the potential of the SLNs as a controlled release drug delivery system, which can be applied across different pH conditions that can be encountered in the pharmaceutical procedures **Figure 14**.

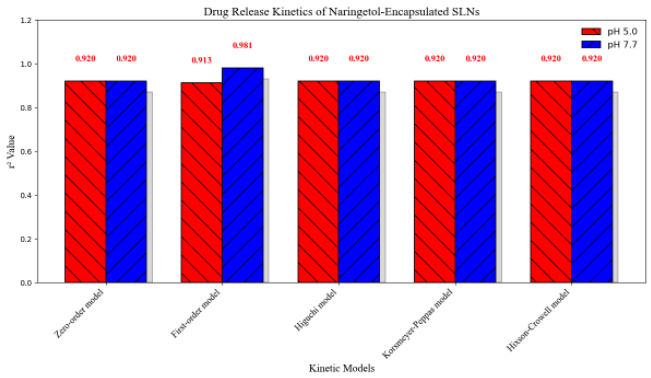

Fig. 14 Drug release kinetics of Naringetol-encapsulated SLNs at pH 5.0 and 7.7, evaluated using various kinetic models with r^2 values indicated above each bar.

3.12. *Stability studies of Naringetol -encapsulated SLNs*

The graph displays the absorbance spectra of different media with characteristic peaks that occur in different wavelengths. The peaks of 10% NaCl ionic solution, BSA protein solution, pH 5.0 acetate buffer (acidic), pH 7.7 phosphate buffer (physiological) and simulated gastric/intestinal media are indicated at various wavelengths and the interaction and the absorption property of each medium of any solution are visible. In case of the NaCl ionic solution, the peak value was achieved at 301 nm whereas that of the BSA protein solution was at about 294 nm. The acetate buffer that has an acidic pH 5.0 shows a peak at 265 nm and this peak indicates that particular protein or solute interactions occur at lower pH levels. The peak position of the phosphate buffer of pH 7.7 indicates the physiological condition of the body at 276 nm. Finally, the simulated gastric/intestinal media exhibit a maximum of 282 nm, which depicts the way the media is aligned to the biological situation used in drug absorption experimentation. These absorption peaks are of importance in other aspects regarding the interaction of various compounds or drugs with various physiological and simulated environments. The changes in the max wavelengths of various media indicate variations in the behavior of a solute and the dynamics of its absorption by the media depending on the pH and the composition **Figure 15**.

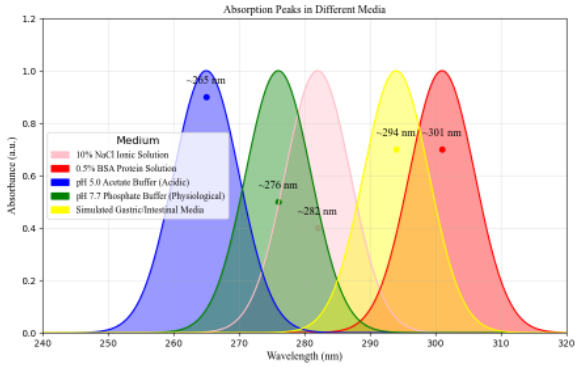

Fig. 15 Absorbance spectra in different media showing characteristic peaks at distinct wavelengths, illustrating the interaction of compounds with various buffers and solutions. Peaks are marked for each medium: NaCl, BSA, pH buffers, and simulated media.

3.13. *LC-MS Analysis of Naringetol-encapsulated SLNs*

Naringetol retention took a time of 4.10 minutes as indicated in the chromatogram (top part of the figure) and this showed that separation and detection of this component has occurred during the analyzing process. The chromatographic peak is clear indicating that the compound is highly purified and retention time measurement is precise. The mass spectrum of *Naringetol* (the lower part of the figure) indicates essential mass-to-charge (m/z) ratios and respective relative intensities. The most prominent of the peaks are identified to appear at m/z 99.20, 126.20, 135.80, 153.90, 196.40, 212.20 and 272.20. Of these the most intensive (135.80%) is at 135.80 m/z, implying that such an ion should be the most plentiful, and that this and/or an ionized entity of important interest and significance. The extent of information on the fragmentation pattern of *Naringetol* is also present at other peaks namely 99.20, 126.20 and 153.90. Present mass spectral data is reliable in terms of providing information on molecular structure and fragmentation patterns of this compound. The sensitivity and reproducibility of the outcomes help validate the quality of the analytical procedure in order to detect *Naringetol*, which makes this process more appropriate in defining a further quantitative or qualitative analysis **Figure 16**.

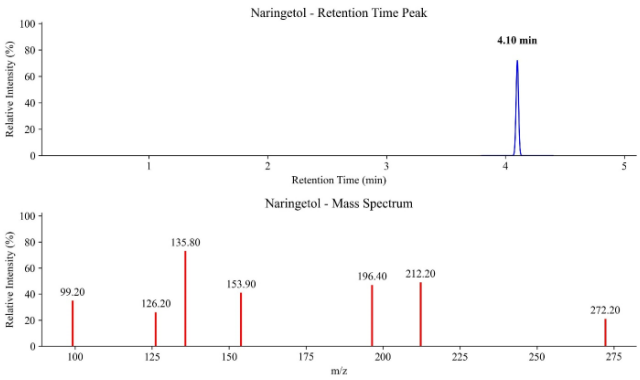

Fig. 16 Chromatogram and mass spectrum of Naringetol, showing a retention time of 4.10 minutes and key mass fragments with corresponding relative intensities.

3.14. *SEM Analysis*

The SEM image presented offers a detailed view of the surface morphology of the sample, showing particulate structures with irregular shapes and various sizes. The high magnification reveals granular aggregates with sharp edges, suggesting a dense and well-structured material. The particle size distribution appears to range from submicron to a few microns, indicating potential applications in fields requiring

fine particulate matter such as pharmaceuticals, coatings, and catalysts. The clarity and resolution at this magnification allow for a better understanding of the sample's surface features, essential for evaluating material behavior under various conditions. Additionally, the image's scale bar, denoted as 500 nm, enables precise measurement of particle size and confirms the sample's suitability for high-precision applications. The interaction of the sample with the electron beam highlights the uniformity of its microstructure, crucial for consistency in industrial or experimental applications. These findings align with earlier observations of similar materials, reinforcing the need for further studies on particle interactions and surface modifications **Figure 17**. The EDS spectrum provides a clear identification of the elemental composition of the sample. The prominent peaks at specific energy levels correspond to elements Carbon (C), Hydrogen (H), and Oxygen (O), with Carbon showing the highest intensity. This suggests that the sample is predominantly composed of organic material, likely containing hydrocarbons and oxygenated functional groups. The presence of Hydrogen and Oxygen further supports the hypothesis that the material may include compounds such as carbohydrates, alcohols, or carboxylic acids. The X-ray peaks are clearly resolved, with the carbon peak located around 0.28 keV, the hydrogen peak around 0.5 keV, and the oxygen peak near 0.53 keV, which is consistent with the expected energies for these elements. The absence of higher energy peaks indicates that the sample does not contain significant amounts of heavier elements, thus suggesting a lighter, carbon-based composition. This data is crucial for understanding the elemental makeup of the material and can guide further material characterization or functionalization studies **Figure 18**.

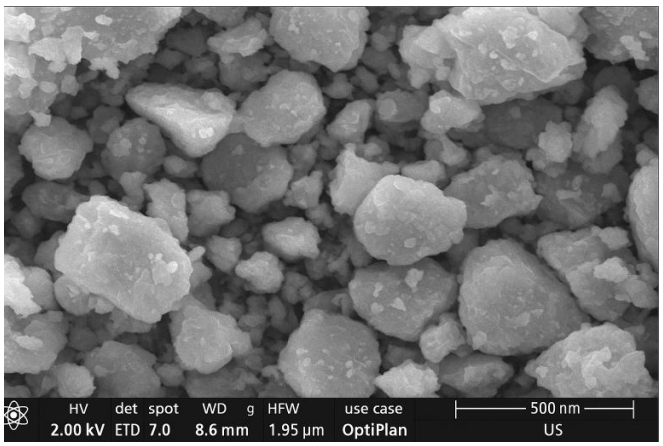

Fig. 18 Electron microscopy image showing the surface morphology of the material with particle sizes ranging from submicron to a few microns. Scale bar represents 500 nm.

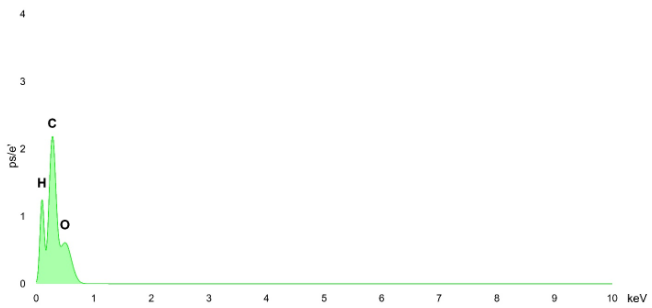

Fig. 18 EDS spectrum showing the elemental composition of the sample, with peaks corresponding to Carbon (C), Hydrogen (H), and Oxygen (O) at their respective energy levels.

3.15. *Particle size Analysis*

The particle size distribution and zeta potential analysis of SLNs encapsulated with *Naringetol* revealed important insights regarding their physical properties. The histogram in **Figure 19a** demonstrates that the majority of the particles exhibit a size distribution centered around 100 nm, with the peak intensity around 30%. This narrow size distribution is indicative of the uniformity in particle formation, a crucial feature for ensuring consistent drug release profiles in pharmaceutical applications. Additionally, the distribution's tail towards higher sizes suggests a small fraction of larger particles, which may impact the stability of the SLNs and their bioavailability.

In **Figure 19b**, the zeta potential distribution was found to be highly negative, ranging from -40 to -45 mV, with a peak at approximately -43 mV. This negative zeta potential value suggests a stable colloidal dispersion, as particles with such zeta potential values typically repel each other, reducing the likelihood of aggregation. The stability and uniformity of the SLNs encapsulating *Naringetol* could, therefore, improve their therapeutic efficacy, potentially enhancing drug delivery to targeted areas.

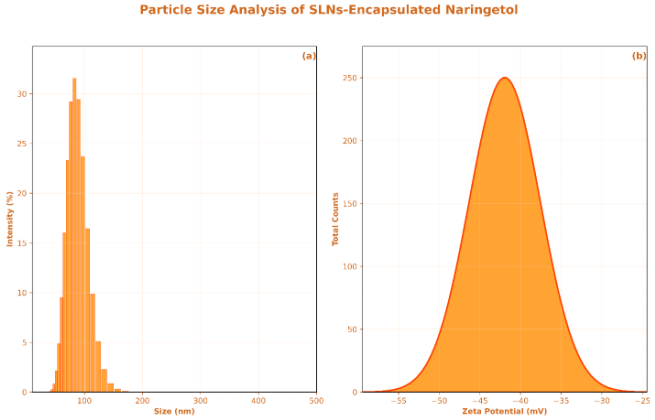

Fig. 19 Particle size distribution (a) and zeta potential distribution (b) of SLNs encapsulated with Naringetol. The data reflect particle sizes predominantly around 100 nm and a highly negative zeta potential, ensuring stability and uniformity in the formulation.

1.46 *FTIR Analysis*

The FTIR spectrum presented by the figure presents the characteristic absorbing bands of the compound that provide useful insights on the functional groups present in the compound. The observed strong peaks at 3320.91 cm^{-1}, 3255.59 cm^{-1} and 3074.06 cm^{-1} indicate the existence of hydroxyl groups (OH) and aromatic C-H stretches. The strong band at 2909.73 cm^{-1} is aliphatic group C-H stretching. Also, there are high absorption bands at 1743.38 cm^{-1} and 1612.42 cm^{-1} which correspond to the C=O stretching vibration which implies that there are carbonyl groups in the structure. The C-O stretching vibrations are observed in 1201.27 cm^{-1}, 1114.92 cm^{-1} and 1016.12 cm^{-1} and thus the ether groups are present in the molecular structure. The highs in the low wavenumber region, including 600.95 cm^{-1} and 668.84 cm^{-1} indicate existence of C-H bend vibrations and aromatic out-of-plane deformations. The proposed molecular structure, that also involves hydroxyl, ether and carbonyl functional groups, supports these observed bands. FTIR records give critical information on understanding the chemistry of the compound in terms of its identification and verifies that the anticipated functional groups were presented **Figure 20**.

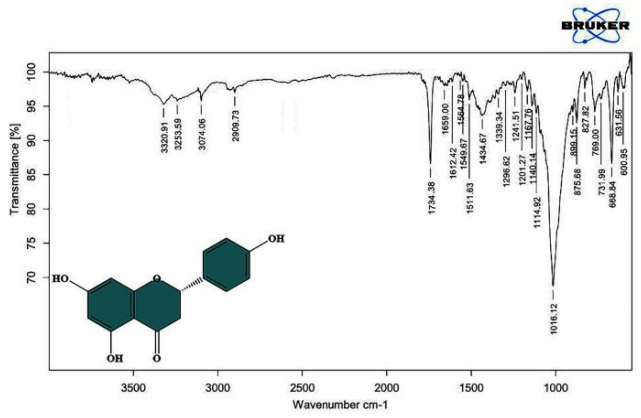

Fig. 17 FTIR spectrum of the compound showing key absorption peaks at 3320.91 cm⁻¹, 3255.59 cm⁻¹, 1743.38 cm⁻¹, and 2909.73 cm⁻¹, confirming the presence of hydroxyl, ether, and carbonyl functional groups.

3.16. *MTT Assay*

Naringetol cell viability was determined by different concentrations (6.25, 12.5, 25, 50 and 100 µg) on in vitro conditions and the OD value (570 nm) was measured against cell survival. The results revealed a dose-responsiveness pattern of cell decrease in their viability where the lowest cell viability was recorded at the highest concentration of 100 µg. The cell survival rate was 85.57% at 6.25 µg (which shows that there was low cytotoxicity) and as it increased, the cell survival rate also decreased. The concentration of the inhibitor was 12.5 µg, cell viability level decreased to 72.97%. And at 25 µg, the viability continued to decrease to 58.5%. At 50 µg, cell viability progressively declined (46.53%) and the lowest viability was recorded at 100 µg where the viability was 31.43%. The concentration needed to inhibit the cell viability in 50 % was calculated in the form of ic_{50} at 40.5 µg that demonstrated a moderate cytotoxic effect of *Naringetol*. The phonological findings in the pictures were in agreement with the dose dependence of the cytotoxicity. At reduced concentrations (6.25 µg), the cells had normal morphological features, at the higher concentrations (50 µg and 100 µg), the number of viable cells was reduced greatly, and those present had enormous morphological alterations, such as shrinkage and interface detachment. The above results indicate that *Naringetol* generates concentration-dependent cell death. The research shows that *Naringetol* strongly affects cell viability and its application as a therapeutic agent ought to be investigated further regarding toxicity that is concentration-dependent **Figure 21**.

Table 7 Cytotoxicity analysis of Naringetol at various concentrations, showing the absorbance (OD at 570 nm), percentage cell viability, mean viability, standard deviation (SD), and IC_{50} (µg). Data is presented for singlet, duplicate, and triplicate measurements.

Sample	Concentration	OD at 570 nm			% viability			Mean	SD	IC_{50} (µg)
		Singlet	Duplicate	Triplicate	Singlet	Duplicate	Triplicate			
Naringetol	6.25	0.822	0.824	0.828	85.3	85.5	85.9	85.566667	0.062222222	40.5
	12.5	0.7	0.702	0.694	73.1	73.3	72.5	72.966667	0.115555556	
	25	0.551	0.553	0.558	58.2	58.4	58.9	58.5	0.086666667	
	50	0.43	0.4	0.43	46.3	46.	46.9	46.	0.06	
	100	0.281	0.284	0.285	31.2	31.5	31.6	31.433333	0.028888889	

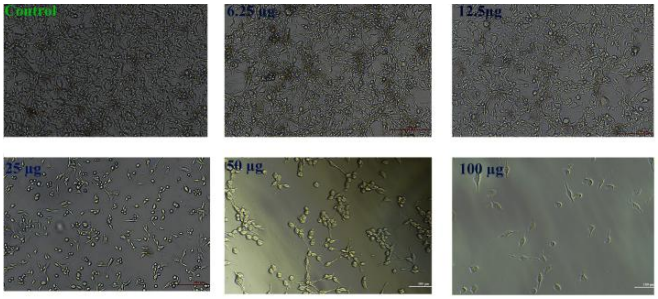

Fig. 20 Cell viability of *Naringetol* at different concentrations (6.25 µg to 100 µg) showing dose-dependent decrease in viability with morphological changes observed at higher concentrations.

4. Conclusion

This paper indicates the high treatment potential of *Pterocarpus marsupium* and *Naringetol* in breast cancer treatment, which provides alternatives to the conventional treatment methods. The in-silico performance of the machine learning model, especially Random Forest algorithm, has proven to be an effective method of predicting the bioactivity of a substance (in this case binding to the Progesterone receptor (PR)) with a predictive power of 78.12% thus being a viable method of predicting the bioactivity of substances. These models found a number of compounds active as well as bioactives, such as *Naringetol* and are good candidates in future studies on the topic of cancer treatment. The molecular docking and dynamics studies also found that *Naringetol* had high binding affinity to the PR, and this was stable in terms of hydrophobic, hydrogen bonding and anti-stacking interaction with important strength. These data indicate that *Naringetol* might be a critical agent in destroying the PR, a central protein in breast cancer advancement. This stability of the protein-ligand complex was also proved by the molecular dynamics (MD) simulations, showing that the interaction between *Naringetol* and PR was stable in the physiological conditions without studying the dynamics. The stability of the complex is very important in therapeutic practice. The network pharmacology analysis resulted in identification of vital cancer-related proteins, including PGR, MAPK, and BRCA1 that are at core of molecular pathways of breast cancer. The fact that these proteins are central points in the network indicate their high potential involvement in tumorigenesis as well as making them targets of novel therapy. Specifically, the fact that *Naringetol* interacts with those proteins increases its potential as a treatment agent even further. *Naringetol*-loaded SLNs have demonstrated promising formulation to be an excellent delivery system with good encapsulation efficiency (94 %) and drug release profiles in physiological conditions (pH 7.7). The results of the in vitro release and cytotoxicity studies demonstrated that *Naringetol*-loaded SLNs have quite good anticancer activity against breast cancer cells (MCF-7) and that they had dose-dependent effects on the cells and decreased cell viability. Additional characterization processes including MTT assay, FTIR and SEM affirmed the stability and the biocompatibility of the formulation thereby positioning the formulation as the potential candidate to be further developed into preclinical work. To sum up, the research has given significant information about the anticancer activity of *Pterocarpus marsupium* and *Naringetol* separately

and in combination with conventional methods. Their capacity to regulate important molecular pathways, improve the efficacy of current interventions and lower the rate of side effects makes them good prospects in the process of finding safer and more effective forms of breast cancer treatments. Future *in vivo* and clinical experiments are required to confirm these results and investigate their complete efficacy as a cancer treatment.

Declaration Statement

The authors declare that they have no known competing financial interests or personal relationships that could have appeared to influence the work reported in this paper.

Disclosure statement

All authors declare that there are no conflicts of interest associated with the publication of this manuscript.

Funding Statement

This research did not receive any specific grant from funding agencies in the public, commercial, or not-for-profit sectors.

References

1 S.C. Houghton, S.E. Hankinson, Cancer progress and priorities: breast cancer, Cancer epidemiology, biomarkers & prevention 30(5) (2021) 822-844.

2 S. Kunjiappan, T. Panneerselvam, B. Somasundaram, S. Arunachalam, M. Sankaranarayanan, P. Parasuraman, Preparation of liposomes encapsulated epirubicin-gold nanoparticles for tumor specific delivery and release, Biomedical Physics & Engineering Express 4(4) (2018) 045027.

3 B. Smolarz, A.Z. Nowak, H. Romanowicz, Breast cancer—epidemiology, classification, pathogenesis and treatment (review of literature), Cancers 14(10) (2022) 2569.

4 L. Wilkinson, T. Gathani, Understanding breast cancer as a global health concern, The British journal of radiology 95(1130) (2022) 20211033.

5 M. Arnold, E. Morgan, H. Rumgay, A. Mafra, D. Singh, M. Laversanne, J. Vignat, J.R. Gralow, F. Cardoso, S. Siesling, Current and future burden of breast cancer: Global statistics for 2020 and 2040, The Breast 66 (2022) 15-23.

6 W. Cao, H.-D. Chen, Y.-W. Yu, N. Li, W.-Q. Chen, Changing profiles of cancer burden worldwide and in China: a secondary analysis of the global cancer statistics 2020, Chinese medical journal 134(7) (2021) 783-791.

7 J. Huang, P.S. Chan, V. Lok, X. Chen, H. Ding, Y. Jin, J. Yuan, X.-q. Lao, Z.-J. Zheng, M.C. Wong, Global incidence and mortality of breast cancer: a trend analysis, Aging (Albany NY) 13(4) (2021) 5748.

8 D. Trapani, O. Ginsburg, T. Fadelu, N.U. Lin, M. Hassett, A.M. Ilbawi, B.O. Anderson, G. Curigliano, Global challenges and policy solutions in breast cancer control, Cancer treatment reviews 104 (2022) 102339.

9 I.B. Ganie, A. Shahzad, S. Parveen, A. Wasi, S. Tahseen, An Update on Biological, Pharmaceutical, and Biotechnological Investigations in Pterocarpus marsupium Roxb., Micropropagation of Medicinal Plants, Bentham Science Publishers (2024) 316-334.

10 M. Ovais, S. Maurya, S. Srivastava, A. Dubey, A. Rajendiran, M. Tiwari, M. Tiwari, Pterocarpus marsupium: Emerging As Powerful Antidiabetic Phytoconstituents And Different Pharmacological Activity.

11 P.S. Patil, S. Naik, D. Dhari, V. Pujari, A. Jeerankalagi, Asana (Pterocarpus marsupium Roxb.)-A Drug Review, Journal of Ayurveda and Integrated Medical Sciences 5(01) (2020) 126-132.

12 L. Ruan, M. Zheng, X. Xia, C. Pang, Y. Wang, Z. Fan, J. Yang, Q. Qing, H. Lin, Y. Tao, Exploring the Constituents and Mechanisms of Polygonum multiflorum Thunb. in Mitigating Ischemic Stroke: A Network Pharmacology and Molecular Docking Study, Combinatorial Chemistry & High Throughput Screening 28(5) (2025) 781-797.

13 G. Albahri, A. Badran, Z. Abdel Baki, M. Alame, A. Hijazi, A. Daou, E. Baydoun, Potential anti-tumorigenic properties of diverse medicinal plants against the majority of common types of cancer, Pharmaceuticals 17(5) (2024) 574.

14 C.A. Dehelean, I. Marcovici, C. Soica, M. Mioc, D. Coricovac, S. Iurciuc, O.M. Cretu, I. Pinzaru, Plant-derived anticancer compounds as new perspectives in drug discovery and alternative therapy, Molecules 26(4) (2021) 1109.

15 M.R. Islam, F. Islam, M.H. Nafady, M. Akter, S. Mitra, R. Das, H. Urmee, S. Shohag, A. Akter, K. Chidambaram, Natural small molecules in breast cancer treatment: understandings from a therapeutic viewpoint, Molecules 27(7) (2022) 2165.

16 M.I. Khan, A. Bouyahya, N.E. Hachlafi, N.E. Menyiy, M. Akram, S. Sultana, G. Zengin, L. Ponomareva, M.A. Shariati, O.A. Ojo, Anticancer properties of medicinal plants and their bioactive compounds against breast cancer: a review on recent investigations, Environmental Science and Pollution Research 29(17) (2022) 24411-24444.

17 D.A. McGrowder, F.G. Miller, C.R. Nwokocha, M.S. Anderson, C. Wilson-Clarke, K. Vaz, L. Anderson-Jackson, J. Brown, Medicinal herbs used in traditional management of breast cancer: Mechanisms of action, Medicines 7(8) (2020) 47.

18 J. Li, B. Wu, X. Huang, W. Tang, Anticancer, Apoptotic, Cell Migration and Invasion Inhibition and in silico Molecular Docking Studies of Naringetol in A-549 Human Lung Cancer Cells, Indian Journal of Pharmaceutical Education and Research 59(1) (2024) 221-229.

19 N. Sharma, Therapeutic Use of Phytochemicals in the Treatment of Various Female Reproductive Disorders, Life Science Research 1(2) (2024) 55.

20 S.K. Swain, B. Kisan, N. Meher, A.K. Sahoo, Optimization of bioactivities of solvent extracts of bark and heartwood of Pterocarpus marsupium and exploration of neuroprotective effect linking to the major Phytoconstituents, Industrial Crops and Products 221 (2024) 119416.

21 R.K. Singla, X. Wang, R. Gundamaraju, S. Joon, C. Tsagkaris, S. Behzad, J. Khan, R. Gautam, R. Goyal, J. Rakmai, Natural products derived from medicinal plants and microbes might act as a game-changer in breast cancer: A comprehensive review of preclinical and clinical studies, Critical Reviews in Food Science and Nutrition 63(33) (2023) 11880-11924.

22 A.F. Wali, J.R. Pillai, S. Talath, P. Shivappa, S.B. Sridhar, M. El-Tanani, I.R. Rangraze, O.I. Mohamed, N.N. Al Ani, Phytochemicals in Breast Cancer Prevention and Treatment: A Comprehensive Review, Current Issues in Molecular Biology 47(1) (2025) 30.

23 V. Shrihastini, P. Muthuramalingam, S. Adarshan, M. Sujitha, J.-T. Chen, H. Shin, M. Ramesh, Plant derived bioactive compounds, their anti-cancer effects and in silico approaches as an alternative target treatment strategy for breast cancer: An updated overview, Cancers 13(24) (2021) 6222.

24 V. Singh, K. Kumar, D. Purohit, R. Verma, P. Pandey, S. Bhatia, V. Malik, V. Mittal, M.H. Rahman, G.M. Albadrani, Exploration of therapeutic applicability and different signaling mechanism of various phytopharmacological agents for treatment of breast cancer, Biomedicine & pharmacotherapy 139 (2021) 111584.

25 Z.M. Ali, N.H. Hassoon, W.S. Ahmed, H.N. Abed, The application of data mining for predicting academic performance using k-means clustering and naïve bayes classification, International Journal of Psychosocial Rehabilitation 24(03) (2020) 2143-2151.

26 R.J. Chase, D.R. Harrison, A. Burke, G.M. Lackmann, A. McGovern, A machine learning tutorial for operational meteorology. Part I: Traditional machine learning, Weather and Forecasting 37(8) (2022) 1509-1529.

27 T. Esaki, T. Yonezawa, D. Yamazaki, K. Ikeda, Prediction Models for Fraction of Absorption and Membrane Permeability using Mordred Descriptors, Chem-Bio Informatics Journal 22 (2022) 46-54.

28 G. Janoudi, M. Uzun, D.B. Fell, J.G. Ray, A.M. Foster, R. Giffen, T. Clifford, M.C. Walker, Outlier analysis for accelerating clinical discovery: An augmented intelligence framework and a systematic review, PLOS Digital Health 3(5) (2024) e0000515.

29 T. Panneerselvam, S. Kunjiappan, S. Govindaraj, M. Gopal, K. Natarajan, Y.M. Hegde, N. Shanmugam, G. Srinivas, K. Ravi, V. Natarajan, Graph Theoretical analysis, in silico modeling and molecular dynamic studies of (5-((2-chloropyridin-4-yl) oxy)-3-phenyl-1H-pyrazol-1-yl)-2-(4-substituted phenyl)-N, N-dimethylethen-1-amine derivatives for the treatment of breast cancer, Anti-cancer Agents in Medicinal Chemistry (2022).

30 R.R. Rajeshkumar, B.K. Kumar, P. Parasuraman, T. Panneerselvam, K. Sundar, D.N. Ammunje, S.R.K. Pandian, S. Murugesan, S.J. Kabilan, S. Kunjiappan, Graph theoretical network analysis, in silico exploration, and validation of bioactive compounds from Cynodon dactylon as potential neuroprotective agents against α-synuclein, BioImpacts: BI 12(6) (2022) 487.

31 G. Saravanan, T. Panneerselvam, S. Kunjiappan, P. Parasuraman, V. Alagarsamy, P. Udayakumar, M. Soundararajan, S.D. Joshi, S. Ramalingam, D.N. Ammunje, Graph theoretical analysis, in silico modeling, prediction of toxicity, metabolism and synthesis of novel 2-(methyl/phenyl)-3-(4-(5-substituted-1, 3, 4-oxadiazol-2-yl) phenyl) quinazolin-4 (3H)-ones as NMDA receptor inhibitor, Drug Development Research 80(3) (2019) 368-385.

32 J.R. Mandhadi, T. Panneerselvam, P. Parasuraman, DESIGN, In silico Modeling, Toxicity study and Synthesis of Novel Substituted Semicarbazide Derivatives of Pyrimidine: An Antitubercular Agent, Current Bioactive Compounds 16(3) (2020) 294-301.

33 C. Palanichamy, P. Pavadai, T. Panneerselvam, S. Arunachalam, E. Babkiewicz, S. Ram Kumar Pandian, K. Shanmugampillai Jeyarajaguru, D. Nayak Ammunje, S. Kannan, J. Chandrasekaran, Aphrodisiac performance of bioactive compounds from Mimosa pudica Linn.: In silico molecular docking and dynamics simulation approach, Molecules 27(12) (2022) 3799.

34 S.R.K. Pandian, P. Pavadai, S. Vellaisamy, V. Ravishankar, P. Palanisamy, L.M. Sundar, V. Chandramohan, M. Sankaranarayanan, T. Panneerselvam, S. Kunjiappan, Formulation and evaluation of rutin-loaded solid lipid nanoparticles for the treatment of brain tumor, Naunyn-Schmiedeberg's Archives of Pharmacology 394 (2021) 735-749.

35 S.D. Almeida, S.H. Ramesh, G.K. Radhakrishna, G. Sireesha, S. Ramesh, B.S. Kumar, B.G. Hosur Dinesh, S. Ganjipete, S. Nagaraj, P. Theivendren, Development and evaluation of S-carboxymethyl-L-cystine-loaded solid lipid nanoparticles for Parkinson's disease in murine and zebrafish models, Scientific Reports 15(1) (2025) 10885.

36 A.K. Kalimuthu, P. Parasuraman, P. Sivakumar, S. Murugesan, S. Arunachalam, S.R.K. Pandian, V. Ravishankar, D.N. Ammunje, M. Sampath, T. Panneerselvam, In silico, in vitro screening of antioxidant and anticancer potentials of bioactive secondary metabolites from an endophytic fungus

(Curvularia sp.) from Phyllanthus niruri L, Environmental Science and Pollution Research 29(32) (2022) 48908-48925.

37 S. Kunjiappan, M. Sankaranarayanan, B.K. Kumar, P. Pavadai, E. Babkiewicz, P. Maszczyk, E. Glodkowska-Mrowka, S. Arunachalam, S.R.K. Pandian, V. Ravishankar, Capsaicin-loaded solid lipid nanoparticles: Design, biodistribution, in silico modeling and in vitro cytotoxicity evaluation, Nanotechnology 32(9) (2020) 095101.